Brownian Motion: An Experimental Study*

Heer Shah and Shwetabh Singh
Ashoka University, Sonepat, Haryana.
(Dated: May 16, 2020)

Abstract: The aim of this project was to investigate Brownian motion in non-spherical particles. For this reason, three particles were chosen namely, peanut, pear, and snowman. The Brownian motion of these particles was investigated under a microscope and video footage of the same was used to determine the mean square displacement against time. Using graphical methods the Diffusion constant for the various particles was determined. The comparison of these values yielded that these observations could be ascribed to some of the geometrical features of the particles in question.

I. INTRODUCTION

This section contains a brief overview of historical developments that underlay the subject of the study. Following this is a discussion on the motivation for this study. Finally, an introduction to the various particles used in the investigation.

A. Historical Development

Brownian motion has been a topic of interest for longer than one would imagine prematurely. In "On the Nature of Things", Lucretius - a Roman poet - ponders upon the nature of the "tiny particles mingling in a multitude of ways" that can be seen suspended in air when sunlight enters through a narrow passage. [1] He concluded that these objects had to be atoms - the indivisible constituents of all matter; with the benefit of hindsight we know that this assertion is a bit removed from the truth. However, motion of tiny suspended particles was already under scrutiny while the Roman empire still stood.

Almost two millennia later, it was a British botanist - Robert Brown, who observed absurd, random motion by suspending pollen grains in water in 1827. At first, he attributed this motion to be a consequence of the fact that these pollen grains were "living". However, when he repeated this experiment with inanimate objects (mainly dust) he observed the same characteristic "random walk". This became a peculiar yet intriguing subject for academics around the world. Nevertheless, for some time, all explanations for this random behaviour fell short of being convincing. Until, eventually, a certain Swiss patent clerk came along and turned this dilemma onto its head. This Swiss patent clerk was none other than Albert Einstein.

Amongst Einstein's four legendary papers from his miracle year (1905) was the Nobel-prize winning marvel on Brownian motion. Einstein pushed for two assumptions: the liquid (water) is made up of atoms, and that these atoms that constitute the liquid are always in motion. Consequently, Einstein expected that the atoms in the liquid would be constantly colliding with the suspended particle. Since the atoms are moving totally arbitrarily in the liquid, the collisions between them and the suspended particle will happen at random causing the suspended particle to undergo random motion.

This discussion; however, has only started to stray away from the ideal, spherical particle in recent times. One can attribute this to notable difficulty that is faced when dealing with the coupled rotational and translational motion that is observed in non-spherical particles. The lack of sufficient experimental data along with the aforementioned theoretical complications have slowed down theoretical progress in this field. With the help of modern instruments it is now possible to investigate this elusive motion experimentally with much greater level of scrutiny and to begin to understand how might the Einstein's model be adapted or altered to serve the purpose of non-spherical particles.

B. Motivation

As discussed above, study of the Brownian motion of non-spherical particles is in its infancy. It is certainly exciting to be able to engage with a topic that is still relatively untouched. Nevertheless, this does not serve as our only motivation to embark on this study. Brownian motion is known to influence trajectories of nanoparticles. These nanoparticles often stray far from the spherical ideal that is considered in Brownian-based models. Furthermore, nanoparticles are thought to be an emerging field of study for medicinal treatments and drug deliverance. Thus, it becomes crucial to be able to understand some peculiarities of its motion. There are various other frontiers in industry where it is important to understand the movement of particles influenced by Brownian forces, while undergoing some flow of its own. The understanding here is only cursory.

* Submitted for the fulfillment of an ISM with the same title

This report seeks to utilize a few examples of non-spherical particles to investigate if some salient features about the Brownian motion of these particular can be established with the help of experimental methods. In the next subsection is a discussion about the good features of the non-spherical particles that have been chosen for the research.

C. Choice of Non-Spherical Particles: Peanut, Pear, and Snowman

Three particle types have been chosen for this investigation. These are non-spherical in nature, yet they are constructed out of spherical elements. This is very helpful. As we will come to learn in Section III, having spherical building blocks makes it possible to model these particle shapes without having to deal with complex shape geometries and configurations. Following are images of each of the particle types:

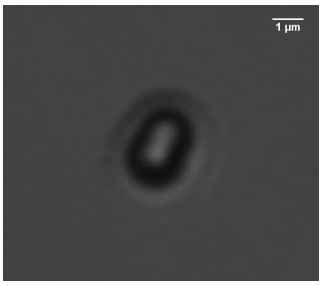

Figure 1. Peanut Particle

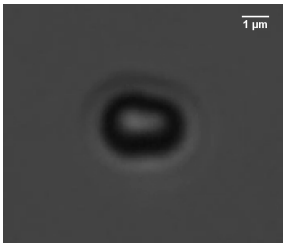

Figure 2. Pear Particle

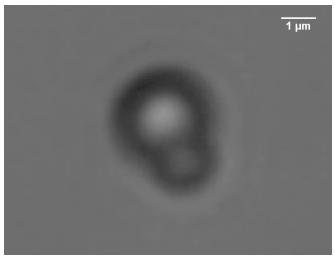

Figure 3. Snowman Particle

II. BACKGROUND LITERATURE

A. Langevin Equation and Brownian Motion

One of the most widely accepted models to explain Brownian motion is the Langevin Model, described by the Langevin Equation and formed by Paul Langevin.

We work with the assumption of Brownian motion being in 1D, and center of mass of particle undergoing the motion described by $x(t)$ at any time t and whose corresponding velocity is $v = \frac{\mathrm{d}x}{\mathrm{d}t}$ and the liquid in which the particle is suspended at an absolute temperature T. Now, considering we can't describe interaction of center of mass with other degree's of freedom, we treat them as constituting a heat reservoir at temperature T and their net effect can be labelled as a force $F(t)$. Now, if we apply Newton's Second Law of Motion, we get:

$$m\frac{\mathrm{d}v}{\mathrm{d}t} = F(t) + G(t) \tag{1}$$

where $G(t)$ is any external force be it gravity, EM force etc. We can observe that due to the nature of the force $F(t)$, it will be a fluctuating force and we can't treat it exactly.

Now, interaction of F(t) with the environment must be in such a way that it always tends to restore the particle to equilibrium and it must be affected by the motion itself. Hence, the net effect force can be decomposed into two parts , $F(t) = F'(t) + F''(t)$ where $F''(t)$ is the rapidly fluctuating part whose average value vanishes and $F'(t)$ is the slowly varying part such that $F'(v) = 0$ in equilibrium when $v = 0$. If we expand $F'(v)$ as a power series when v is not too large, we get the linear term in v as the non vanishing term, hence the non vanishing part must have the general form:

$$F'(t) = -\alpha\bar{v} \tag{2}$$

Thus we can write:

$$m\frac{\mathrm{d}v}{\mathrm{d}t} = F''(t) + G(t) - \alpha v \tag{3}$$

This is the Langevin Equation and we can now use it to find mean square displacement. In the absence of any external force, which is where are sample is, the equation becomes:

$$m\frac{\mathrm{d}v}{\mathrm{d}t} = F''(t) - \alpha v \tag{4}$$

Assuming the particles to be spherical, we apply Stokes law and by comparison with the frictional force, we get $\alpha = 6\pi\eta a$, where a is the radius of the sphere. Now we consider the case of thermal equilibrium, where due to random motion and by symmetry arguments, the mean displacement of particle can be taken as 0, thus we try to calculate the mean square displacement. To do this, we take the Langevin Equation (4) and multiply both sides by x, we get:

$$mx\frac{\mathrm{d}\dot{x}}{\mathrm{d}t} = m(\frac{\mathrm{d}x\dot{x}}{\mathrm{d}t} - \dot{x}^2) = -\alpha x\dot{x} + F''(t)x \tag{5}$$

Then we take average of both sides and use the equipartition theorem to get:

$$m\left\langle \frac{\mathrm{d}(x\dot{x})}{\mathrm{d}t} \right\rangle = m\frac{\mathrm{d}\left\langle x\dot{x}\right\rangle}{\mathrm{d}t} = kT - \alpha\left\langle x\dot{x}\right\rangle \tag{6}$$

This is a simple differential equation in $\langle x\dot{x}\rangle$ and can be solved to get

$$\langle x\dot{x}\rangle = Ce^{-\gamma t} + \frac{kT}{\alpha} \tag{7}$$

where C is just a constant and $\gamma = \frac{\alpha}{m}$. Assuming at t = 0, every particle starts out at x = 0, so that x can give us displacement, we get $C = -\frac{kT}{\alpha}$ and thus we can write:

$$\langle x\dot{x}\rangle = \frac{1}{2}\frac{\mathrm{d}\left\langle x^2\right\rangle}{\mathrm{d}t} = \frac{kT}{\alpha}(1 - e^{-\gamma t}) \tag{8}$$

Integrating gives us

$$\left\langle x^2\right\rangle = \frac{2kT}{\alpha}(t - \frac{1}{\gamma}(1 - e^{-\gamma t})) \tag{9}$$

And if we apply the long time approximation, $t \gg \frac{1}{\gamma}$, then $e^{-\gamma t} \to 0$, and thus (9) becomes

$$\left\langle x^2\right\rangle = \frac{2kT}{\alpha}t = 2Dt \tag{10}$$

We can redo the calculation for $\left\langle y^2\right\rangle$ and get the 2D mean square displacement as $\left\langle r^2\right\rangle = 4\mathrm{Dt}$.[2] This is the mean square displacement according to Langevin Equation.

B. Einstein's Model for Spherical Particles

As described earlier, Einstein's model of the Brownian motion involves collisions between atoms or molecules, and the suspended particle. One would be tempted to think that since we are dealing with collisions of bodies classical mechanics would help us solve this problem. However, the number of collisions that occur each second are too great for calculation by hand. Therefore, Einstein chose to take an aggregate approach: to consider the collective motion of all atoms.

First we will start by considering Brownian motion along a single dimension (x), which can then easily be adjusted to achieve the expression for 3-dimensional motion. Einstein considered the motion of the particle in x over a time period τ. **Note:** Coordinates are to be chosen so that the suspended particle lies at the origin at time, t = 0. He further went onto say that this motion can characterized by a probability density function $\varphi(\Phi)$, where Φ is a random variable. As a result, we can do a Taylor series expansion of the density function (ρ) around $t + \tau$. This goes as follows:

$$\begin{aligned}\rho(x, t+\tau) &= \rho(x,t) + \tau\frac{\partial\rho(x)}{\partial t} + \tau^2\frac{\partial^2\rho(x)}{\partial t^2} + \cdots \\ &= \int_{-\infty}^{+\infty}\rho(x-\Phi, t)\varphi(\Phi)d\Phi. \end{aligned}\tag{11}$$

A Taylor expansion on the right hand side around $\rho(x - \Phi)$ yields:

$$\begin{aligned}\rho(x,t+\tau) = \rho(x,t)&\int_{-\infty}^{+\infty}\varphi(\Phi)d\Phi \\ -\frac{\partial\rho(x,t)}{\partial x}&\int_{-\infty}^{+\infty}\Phi\varphi(\Phi)d\Phi \\ +\frac{\partial^2\rho(x,t)}{\partial x^2}&\int_{-\infty}^{+\infty}\frac{\Phi^2}{2}\varphi(\Phi)d\Phi - \cdots\end{aligned}\tag{12}$$

Now, $\int_{-\infty}^{+\infty}\varphi(\Phi)d\Phi$ is an expression for the probability over the entire space, which is by definition equal to 1. On the other hand, $\int_{-\infty}^{+\infty}\Phi\varphi(\Phi)d\Phi$ is known to be 0, because of the symmetry of the problem: it is equal to $< \Phi >$. Thus, we are left with the following:

$$\rho(x,t+\tau) = \rho(x,t) + \frac{\partial^2\rho}{\partial x^2}\int_{-\infty}^{+\infty}\frac{\Phi^2}{2}\varphi(\Phi)d\Phi + \mathcal{O}(\frac{\partial^{(n)}\rho}{\partial x^{(n)}}) \tag{13}$$

If we ignore the higher order terms, an equation of this form emerges:

$$\frac{\rho(x,t+\tau) - \rho(x,t)}{\tau} = \frac{\partial\rho}{\partial t} = \frac{\partial^2\rho}{\partial x^2}\int_{-\infty}^{+\infty}\frac{\Phi^2}{2\tau}\varphi(\Phi)d\Phi \tag{14}$$

the second moment of probability of displacement Φ : $\int_{-\infty}^{+\infty} \frac{\Phi^2}{2\tau}\varphi(\Phi)d\Phi$, is interpreted as the mass diffusivity, D, of the equation.

Then, the density of Brownian particles ρ at point x at time t satisfies the diffusion equation:

$$\frac{\partial \rho}{\partial t} = D\frac{\partial^2 \rho}{\partial x^2} \tag{15}$$

The solution to the diffusion equation is equal to (in the normalized form):

$$\rho(x,t) = \frac{1}{\sqrt{4\pi Dt}} e^{\frac{-x^2}{4Dt}} \tag{16}$$

This expression (a normal distribution) allowed Einstein to calculate the moments directly. The first moment vanishes, meaning that the Brownian particle is equally likely to move to the left as it is to move to the right. The second moment does not vanish and gives: $\langle x^2 \rangle = 2\mathrm{Dt}$.

Now, a similar equation can be arrived at for motion in any number of dimensions, by realising that the diffusion equation is just going to have a Laplacian with the additional directions. The coefficient to the solution will be multiplied with itself in 2-D motion, which gives us the following:

$$\rho(x,y,t) = \frac{1}{\sqrt{4\pi Dt}} e^{\frac{-(x^2+y^2)}{4Dt}} = \frac{1}{4\pi Dt} e^{\frac{-r^2}{4Dt}} \tag{17}$$

So, consequently the second moment leads us to following relation: $\langle r^2 \rangle = 4\mathrm{Dt}$. [3]

C. The Ergodic Hypothesis

The Ergodic hypothesis implies that, over long periods of time, the time spent by a system in some region of the phase space of microstates with the same energy is proportional to the volume of this region, i.e., that all accessible microstates are equiprobable over a long period of time.

This implies that if the Brownian particle is observed in motion long enough, it is probable that it will adopt all the possible instantaneous velocities. As opposed to one particle, one could measure the the instantaneous velocity of a large number of particles for one time step and average it: this is referred to as the ensemble average. The Ergodic hypothesis indicates to us that these two methods are equivalent.

The consequences of this widely-recognized hypothesis allow the experiment to be undertaken using the time average method, which does not require that one analyze a large number of particles but just a few particles for long time periods. This makes it possible to conduct the experiment effectively with the limited resources that are available.

III. MODELLING THE NON-SPHERICAL PARTICLES

In order to appropriate any observations to the shape and characteristics of the particular particle, it is important to construct a model of the particle in question. This would require that a few assumptions be made about the particle for the purpose of efficiency and efficacy. The following subsection addresses this matter explicitly.

A. Assumptions

The manufacturer of the particles provides only the most cursory information about the dimensions and the nature of the particle. The length and breadth of the particle (maximal values) are provided to serve as information about its dimensions. Apart from this the name of the particles is supposed to as some description about the shape. However, none of the names translate to any insight into the geometry of the shape.

Nevertheless, with a few simple (and very apt) assumptions it is possible to make use of this limited information and some imaging tools to construct a reliable model of the shape. From images provided earlier (FIG 1,2,3) one can see that shapes are somewhat spherical. It is this that which we use to our advantage. Each of the three shapes can be considered to be composed of two spheres, which are not necessarily of the same size. The observed shape could be considered as a result of these spheres intersecting. Thus, the first assumption is that the shapes are constructed from spherical constituents. Towards the end of this section, it will be verified that - for most part - this is a perfectly sound assumption to make.

Next, we assume that the particle is rigid, at least rigid enough that the forces experienced during Brownian motion do not significantly deform it. For the purpose of investigating Brownian motion, this is a very usual assumption to make. Nonetheless, it is better to explicitly recognize the inherent assumptions in a study.

Video evidence would suggest that this is also a perfectly based assumption to make.

Lastly, we assume that the particle is homogeneous in its composition, i.e. it has uniform density. This is very difficult to verify; however, this is a necessary assumption. Without this condition it would be difficult to ascribe any findings of this study to the shape of the particles. Of course this is also a common assumption that would be made in a study on Brownian motion.

B. Common Chord Method

Since intersecting spheres are being considered, the exact parameters the region that it missing from the sphere need to be determined. This can be done by considering the plane along which the line segment joining the two centers of the spheres lay. We can consider the surface of the spheres in this plane to be circles. Since the two centers are connected by a line segment along this region, the circles considered here would have the same diameter as the spheres. Therefore, the diagram would appear as follows:

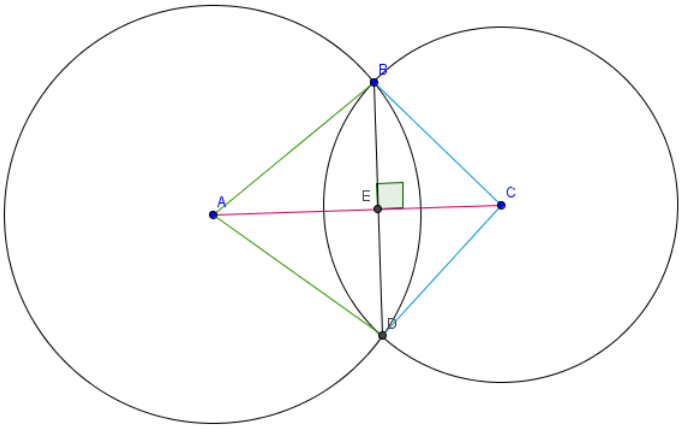

Figure 4. Illustration of the Intersecting Circles

This diagram shows that what is being observed is the common chord of two circles. The line segments AB = AD represent the radius of the circle on the left. Similarly, segments BC = DC represent the radius of the circle on the right. Therefore, if the length BD (Note: 2BE = 2ED = BD) is measured on an image analysis software along with the diameters of the supposed spheres (to get the radius), the following expressions (from Pythagoras' theorem) can be used to determine the relevant quantities:

$$AE = \sqrt{(AB)^2 - (BE)^2} \tag{18}$$

$$CE = \sqrt{(CB)^2 - (BE)^2} \tag{19}$$

C. The Spherical Cap

The previous sub-section allows one to determine the plane of intersection for the two spheres; however, this is not enough. The previous sub-section makes it possible to construct the physical model itself, but beyond this the area and volume calculations are also important. To achieve this, the volume of the "missing" regions from the spheres must be determined. The shape of these regions is referred to as spherical caps. By using the function of rotation of a spherical cap, it is possible to determine the volume and area of this region:

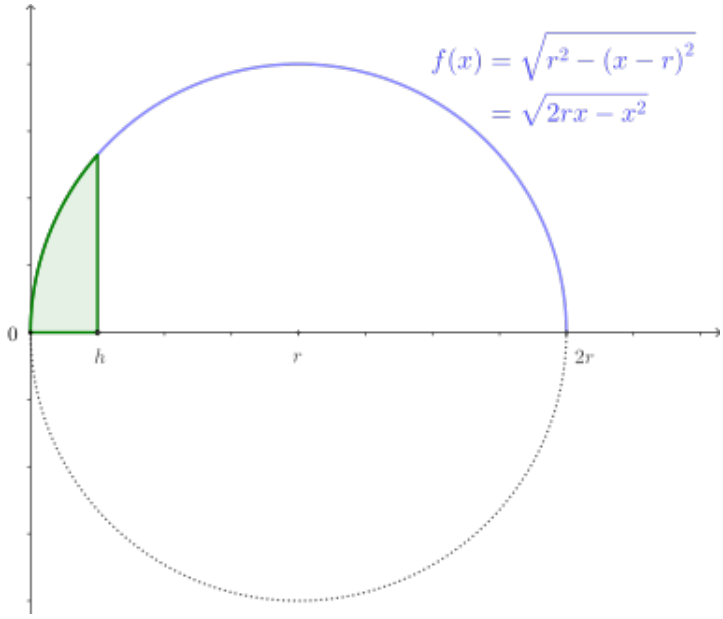

Figure 5. Illustration Showing the Function of rotation for a Spherical Cap

The function of rotation can be expressed as follows:

$$f(x) = \sqrt{r^2 - (x-r)^2} = \sqrt{2rx - x^2},\ x \in [0, h] \tag{20}$$

The area of the surface of rotation is expressed in the following manner:

$$A = 2\pi \int_0^h dx f(x)\sqrt{1 + f'(x)} \tag{21}$$

In this case, $f'(x)$ is as follows:

$$f'(x) = \frac{r-x}{\sqrt{2rx-x^2}} \tag{22}$$

Therefore, the area is as follows:

$$A = \pi \int_0^h dx\sqrt{2rx-x^2} \times \frac{r^2}{\sqrt{2rx-x^2}} = \pi \int_0^h dxr = 2\pi rh \tag{23}$$

The volume of the solid of revolution is expressed in the following manner:

$$V = \pi \int_0^h dx f(x)^2 \tag{24}$$

Thus, the volume of the spherical cap is:

$$V = \pi \int_0^h dx \left(\sqrt{2rx-x^2}\right)^2 = \pi \left[rx^2 - \frac{x^3}{3}\right]_0^h = \frac{\pi h^2}{3}(3r-h) \tag{25}$$

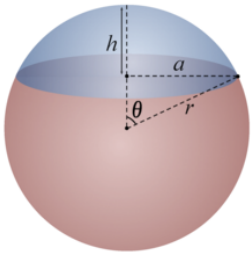

Figure 6. Spherical Cap: The Solid of Revolution [In Blue]

With this the volume of the individual spheres (with the caps removed) can be determined, and the total of the two spheres gives us the volume of the particle.

D. Finding the Relevant Quantities from Images

As referenced before, some quantities need to be determined using an image analysis software. The process requires more time and effort then would seem apparent. FIG 7. would help explain the steps undertaken:

The red and the blue tape (Tape A and Tape C) represent the length and the breadth measurements,

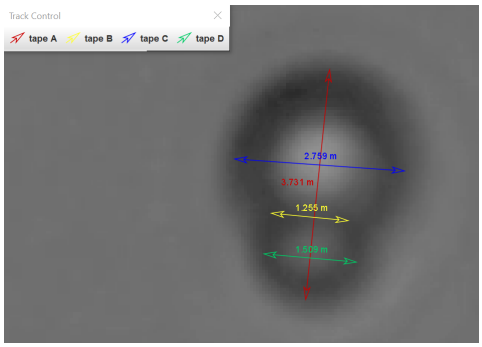

Figure 7. Snowman Image Analysis

respectively. The breadth measurement is the same as the diameter of the larger circle, because that would define the maximum breadth any element in the shape could reach. The yellow tape (Tape B) represents the length of the boundary of the intersection. Finally, the green tape (Tape D) represents the diameter of the smaller circle.

Nevertheless, this one measurement is not all that needs to be taken for the result. The image is from one of the images of the Snowman particle from the videos. At any given instant the particle is not necessarily in the configuration where the plane of observation is perpendicular to its axis. Therefore, in order to truly capture the values of these quantities, a lot of readings are taken and then the maximal values are utilized to determine the quantities in question.

E. The Results of Modelling

1. *Peanut Particle*

The following were the values determined to correspond to the Peanut Particle:

1. Length: 2.703 ($\pm$0.001) μm
2. Width: 1.792 ($\pm$0.001) μm
3. Diameter 1: 1.796 ($\pm$0.001) μm
4. Diameter 2: 1.796 ($\pm$0.001) μm
5. Length of Shared Region (AE + CE): 0.896 ($\pm$0.002) μm
6. Volume: 5.15 μm^3
7. Surface Area: 15.24 μm^2

The following Figures show the model that was developed [Lengths in FIG. 8 are rounded to 1 d.p.]:

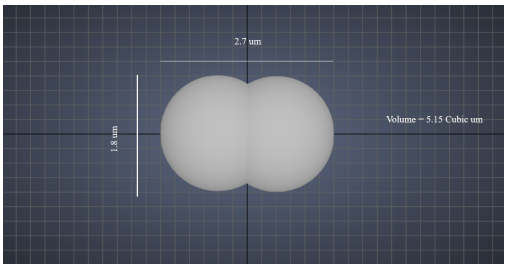

Figure 8. Labelled Scale Model of Peanut

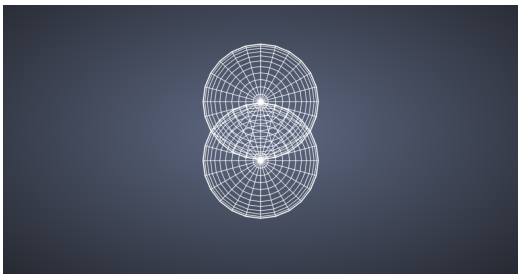

Figure 9. Mesh Diagram Representing Peanut

2. *Pear Particle*

The following were the values determined to correspond to the Pear Particle:

1. Length: 3.197 ($\pm$0.001) μm
2. Width: 2.600 ($\pm$0.001) μm
3. Diameter 1: 2.600 ($\pm$0.001) μm
4. Diameter 2: 2.505 ($\pm$0.001) μm
5. Length of Shared Region (AE + CE): 1.650 ($\pm$0.002) μm
6. Volume: 13.11 μm^3
7. Surface Area: 27.71 μm^2

The following Figures show the model that was developed [Lengths in FIG. 10 are rounded to 1 d.p.]:

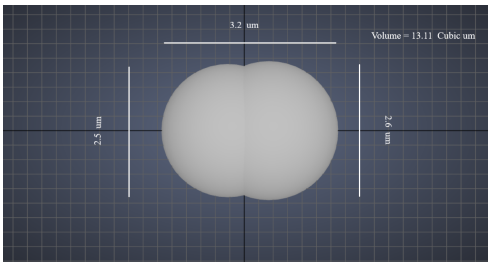

Figure 10. Labelled Scale Model of Pear

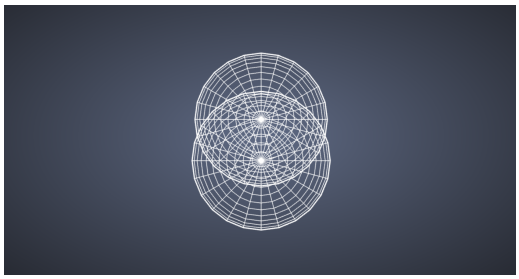

Figure 11. Mesh Diagram Representing Pear

3. *Snowman Particle*

The following were the values determined to correspond to the Snowman Particle:

1. Length: 3.799 ($\pm$0.001) μm
2. Width: 2.813 ($\pm$0.001) μm
3. Diameter 1: 2.813 ($\pm$0.001) μm
4. Diameter 2: 1.502 ($\pm$0.001) μm
5. Length of Shared Region (AE + CE): 0.507 ($\pm$0.002) μm
6. Volume: 12.94 μm^3
7. Surface Area: 29.06 μm^2

The following Figures show the model that was developed [Lengths in FIG. 12 are rounded to 1 d.p.]:

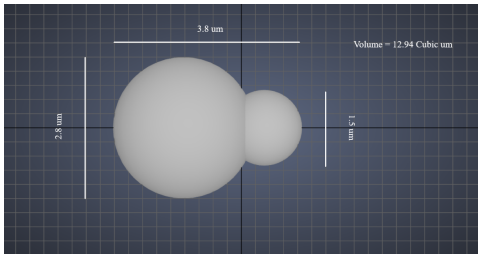

Figure 12. Labelled Scale Model of Snowman

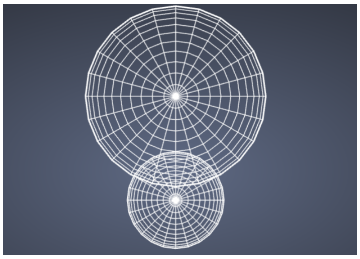

Figure 13. Mesh Diagram Representing Snowman

F. Verifying Obtained Results

There is a way to verify the results obtained in this investigation. Firstly, the manufacturers provide the length and width measurements. Apart from this it is possible to get a confirmation on the length on the shared region. In the previous section, the length of AE and CE are used to determine that value; however, the shared length is also equal to (Diameter 1 + Diameter 2) - Length.

All the length and width measurements are extremely close to the quoted values. That is also true for most of the shared region lengths. However, the length of the shared region in the pear particle turns out to be slightly off (that is why it coloured in red):

$$AE + CE = 1.650\ (\pm 0.002)\ \mu m \tag{26}$$

$$\text{(Diameter 1 + Diameter 2) - Length} = 1.908\ (\pm 0.003)\ \mu m \tag{27}$$

Therefore, there is a significant difference in the two values. This would approximately translate to an 8 % deviation in the total length of the particle: orders of magnitude larger than that of the other particle's errors.

G. Understanding the Deviation

The fact that all the other measurements for the other particles were very accurate allows us to cast doubt away from the means used to arrive at the values. The only other reasonable explanation for the deviation is that the two constituent elements are not necessarily spherical. In this case, the diameter measurement would not accurately reflect the length that should be missing: exactly what is observed here.

This brings forth the question about whether it is reasonable to continuity with the assumption that the particle is composed of intersecting spheres. Nevertheless, the other option would be to employ an ellipsoid or some more complicated shape. The accuracy might increase, but the ability to calculate various quantities and to make connections to what is previously known. Here it is critical to preserve simplicity. The deviation is small enough that one can continue using the spherical model.

IV. METHODOLOGY

In order to conduct this study, it is important that the sample preparation and subsequent recording and viewing be done in a certain way. The following subsections cover these methods.

A. Sample Preparation

1. Making the Solution

The sample in its barest essence is just a containment chamber to hold a specific quantity of sample solution. The manufacturer provided solutions(hereon referred to as base solutions) were diluted twice to obtain the working solution.

The first dilution was 1 ml of base solution in 50ml of distilled water, this was labelled Master solution, as in case working solution was completely spent or second dilution was not up to satisfactory levels, this would be used to re-prepare rather than the base solution. The first dilution was also done under the direct supervision of Professor Pramoda.

The second dilution was done by taking 4ml of master solution in 4ml of distilled water. The process was repeated for all three particle types. These solutions were appropriately shook every time before a sample was prepared to ensure uniform density.

2. Glass Slide Creation

A standard microscopic glass was used as a base to create the sample. The containment chamber or "the chamber" was prepared from an Aluminum tape. A small rectangular/square strip of Aluminum tape was cut and a hole was punched in it using a Kangaro DP600 punch machine. The hole diameter was of 5.5mm. Below is an image attached of a sample chamber from Aluminum tape.

Figure 14. Chamber from Aluminum tape

After the chamber is stuck to the slide, it was ensured that there were no air bubbles between the surfaces. After removing any air bubbles encountered, a small droplet was put in the middle of chamber and immediately covered with a glass cover slip. The cover slip was put on top keeping any air bubbles out and ensuring no overflow of liquid from the chamber happened. After ensuring the absence of both the spillage and air bubbles, finally the chamber was sealed using nail polish. Nail polish was put all around the cover slip, so as to keep the cover slip in place and prevent any movement of air that might dry up the liquid in sample.

Figure 15. Typical Sample ready for viewing

B. Microscope Assembly

The primary microscope used in this investigation was assembled specifically for the purpose of this investigation. This was so because, to conduct a Brownian motion experiment it is necessary that the vibrations experienced by the sample are minimal. To achieve this an anti-vibration table was used, and so a microscope has to be assembled over it.

The microscope objective along with the camera were positioned vertically with the use of a stand and clamps over a honeycomb tabletop to keep the device fixated in position. The main body of the camera and the objective were attached to an XY moving platform to adjust position in the direction parallel to the sample, and the clamp had a rotating mechanism which allowed adjustment of position perpendicular to the sample (z-direction).

An external light source was used to provide sufficient light for the observations to be made. A platform for putting the sample was made using a laser mount. A laser mount was chosen, because it allowed us to make minute corrections in the level of the platform, which made it possible to eliminate any effects of drift on the sample. Following is an image of the setup:

The choice of the microscope objective was very critical for the process. The objective, firstly, needed to have a sufficient magnification factor that would enable

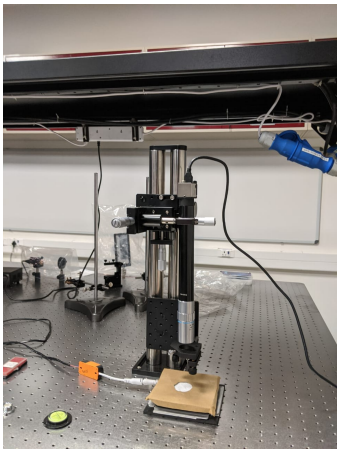

Figure 16. Assembled Microscope

the various elements of the particle to be distinguished during image analysis procedures. Thus, an objective with a 50X magnification factor was selected. However, this is not the extent of features that are desired from a lens.

The microscope used for this investigation was Metallographic (Indicated by **M** in FIG 17). This type of microscope employs vertical illumination, in which the light source is inserted into the microscope tube below the eyepiece by means of a beam splitter. Light shines down through the objective and is focused through the objective onto the specimen. The light reflected or scattered back to the objective is then imaged back at the eyepiece. In this manner, opaque objects such as metals can be examined under the microscope. In this experiment, this allows for the opaque particles to be observed.

The microscope used for this investigation was also Apochromatic (Indicated by **Apo** in FIG 17). An Apochromatic lens is a lens that has better correction of chromatic and spherical aberration than the much more common achromatic lenses. Chromatic aberration is the phenomenon of different colors focusing at different distances from a lens, and this lens corrects for this error. Apochromatic lenses are designed to bring three wavelengths (typically red, green, and blue) into focus in the same plane.[4] The residual color error (secondary spectrum) can be up to an order of magnitude less than for an achromatic lens of equivalent aperture and focal length. Apochromats are also corrected for spherical aberration at two wavelengths, rather than one as in an achromat. This feature helps colour contrast to be used for determination of the particle boundary and reduce error from different focusing distances.

Finally, the microscope also had Flat Field correction (Indicated by **Plan** in FIG 17). Flat fielding refers to the process of compensating for different gains and dark currents in a detector. Once a detector has been

appropriately flat-fielded, a uniform signal will create a uniform output (hence flat-field). This then means any further signal is due to the phenomenon being detected and not a systematic error.[5] Similar to the Apochromatic correction, this feature helps colour contrast to be used for determination of the particle boundary and reduce errors by cancelling the effects of image artifacts caused by variations in the pixel-to-pixel sensitivity of the detector and by distortions in the optical path.

Following is an image a microscope objective with some similar characteristics which have been discussed in the previous few paragraphs:

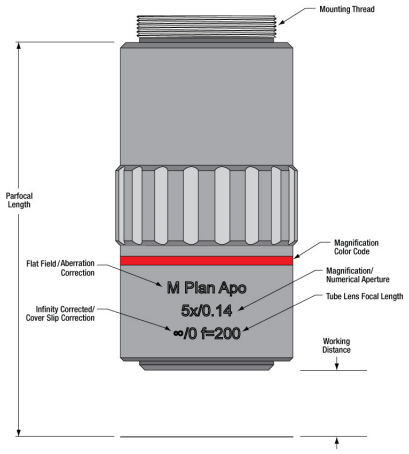

Figure 17. A Metallographic, Apochromatic, and Flat Field correction Microscope Objective

C. The Alternate Microscope

Apart from the microscope that was assembled for this experiment, there was a microscope that was also utilized. This microscope has already been constructed previously, and had a higher lenses with much greater magnification. This microscope was utilized to take images that would be more useful in taking measurements from the particles. That it to say, that FIG. 7 is a product of this microscope. The larger magnification allows for more accurate measurements to be taken. Following is a schematic diagram of the microscope in question:

D. Viewing and Recording

Since there were two separate microscopes used at different points in the investigation, two different soft-

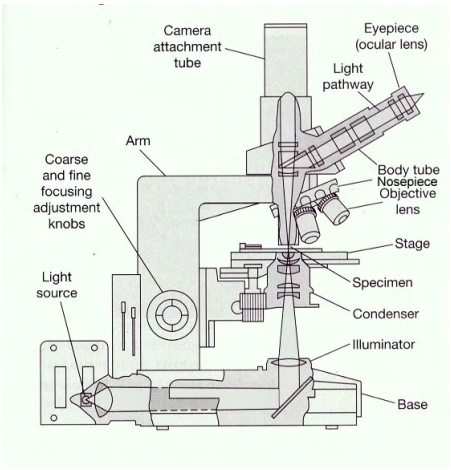

Figure 18. Labelled Microscope Schematic Diagram

ware applications were used to undertake the necessary observations and recordings.

For the first microscope, which was assembled, Micro-Manager^{TM} was the software employed. The second time around the software used was in compliance with the manufacturer of the microscope: Leica Microsystems. This was the proprietary software made to assist analysis of images from the particular microscope.

Note: Before positioning the slide upon the platform it is ensured that the platform is parallel to the ground using a spirit level.

A relevant section of the slide was then focused on, an area not too high and too low in particle density was chosen as the subject of study is diffusivity of individual particles and hence in-particle collision is not desired, which increases with increase in the local density. Too low particle density would prompt more recording to be done, which would require more time and sample preparation, thus to be economical in our approach, an area with about 7-15 particles was chosen and accordingly recorded.

More details about these software can be found in the Appendix.

E. Precautionary Measures

The experiment is sensitive to very small inconsistencies and a host of exterior phenomena, as is suggested by the need to use nail polish to seal the chamber. Thus, it becomes all the more important to avoid errors that can easily be picked out before the experiment and help avoid glaring errors in the results. Following are some of the measures that were taken to improve accuracy of results:

1. Check for fluid leaks or air-bubbles in the sample, it is usually very difficult to get rid of them without unsettling something else. So, one must ensure that none are formed when making the slide.

2. The set up is very sensitive to external disturbances - even your footsteps. So while recording the video, try to minimize these as much as possible. All this had to be taken in consideration despite the fact that we had an anti-vibration table.

3. The results of the experiment are very sensitive to changes in temperature. A thermostat was used to control the temperature. It was found that the fell between between the following range during the investigations: $24(\pm 0.5)^\circ$ C

V. DATA ANALYSIS

A. Extracting Data from the Videos and Images

The data from the recorded images(in .tiff format) was extracted using ImageJ applet connected to Micro-Manager^{TM}. The Manual tracking plugin was used to track the relevant particles. A screenshot of the UI is attached below. The plugin lets the user track any desired point by pointing and clicking throughout the length of image/video.

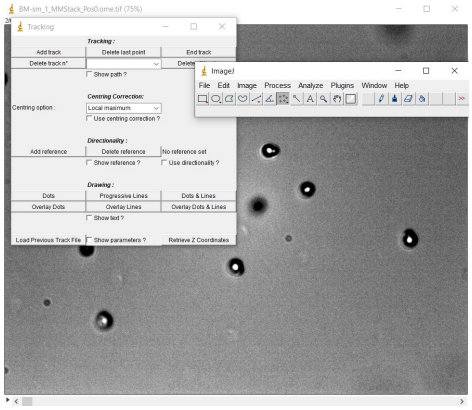

Figure 19. UI of ImageJ applet used to extract data

B. Processing Extracted Data

The data collected from videos was stored as comma separated values. The data collected conveyed the x and y position of the centre of mass at any given time stamp. A python program was used to convert this information into the required parameters for successful analysis.

The method used to analyze the Brownian motion of the particles is the time-step increment method. In the time-step increment method, the data set is treated so that there are n different variations (n equals the number of total time steps) with time-step length varying from 1 to n. The ¡ r^2 ¿ value is calculated for the entire range of data for each set of time-steps, and the ¡ r^2 ¿ values are plotted against the corresponding time-step length. The data set is then treated to a linear fitting algorithm to determine the slope of the graph, which allows the diffusivity of the particle to be inferred. The python code for the same can be found in the appendix.

C. Results

1. *Peanut Result Graphs*

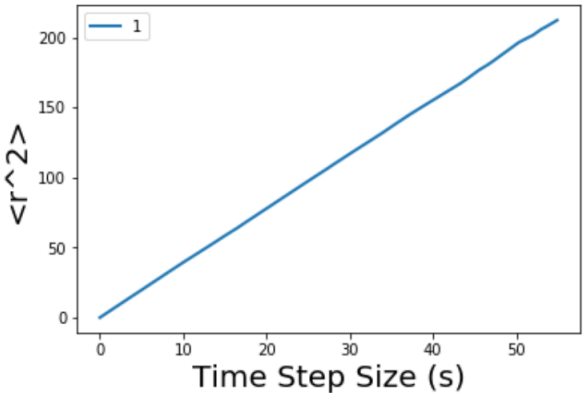

Figure 20. Graph Displaying Mean Square Displacement against Time Step size for Peanut Particle

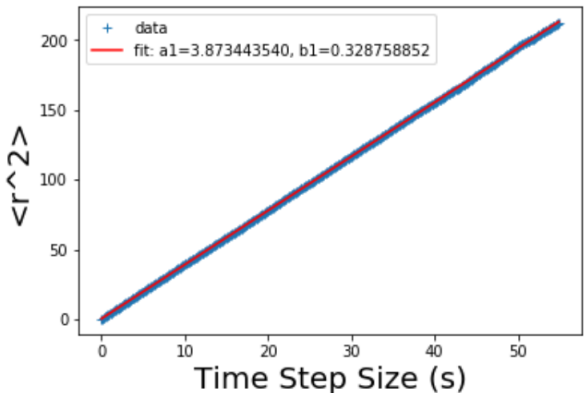

Figure 21. Graph Displaying Mean Square Displacement against Time Step size for Peanut Particle along with Linear Regression

2. *Pear Result Graphs*

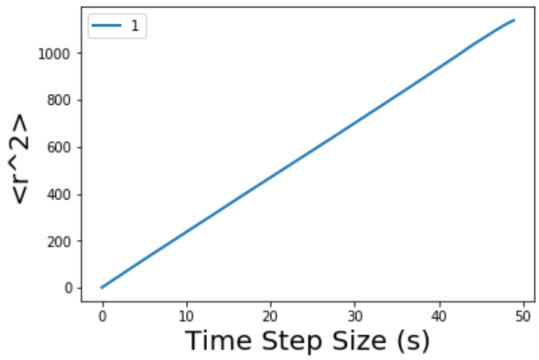

Figure 22. Graph Displaying Mean Square Displacement against Time Step size for Pear Particle

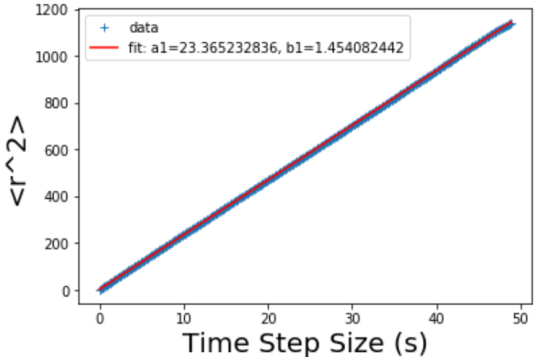

Figure 23. Graph Displaying Mean Square Displacement against Time Step size for Pear Particle along with Linear Regression

3. *Snowman Result Graphs*

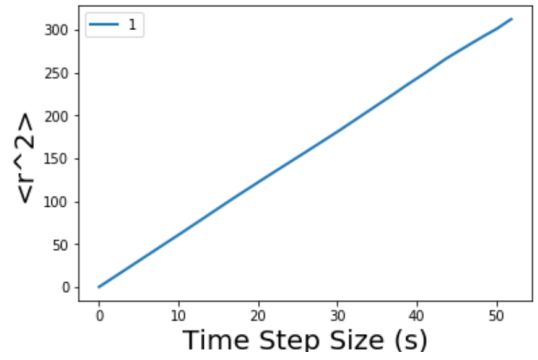

Figure 24. Graph Displaying Mean Square Displacement against Time Step size for Snowman Particle

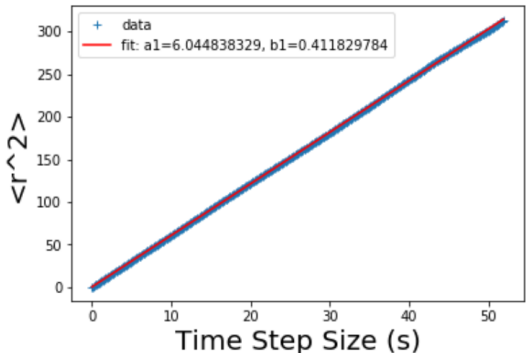

Figure 25. Graph Displaying Mean Square Displacement against Time Step size for Snowman Particle along with Linear Regression

D. Interpreting the Results

The quantity a1 that is used for labelling in each of the linear regression graphs in the previous sub-section refers to the slope of the plotted curve determined using linear fitting. These values directly correspond to 4D according to the background literature provided in section II. Consequently, Table I. presents the values of diffusion constant (D) of each of the particles (values have a factor $10^{-12}\frac{m^2}{s}$ multiplied to them):

Table I. Particle Diffusion Constant

Sr. No	Name of Particle	Diffusion Constants
1	Peanut	0.968
2	Pear	5.841
3	Snowman	1.511

Diffusion constants are definitely dependent on the surface area of the particles. This is one variable that is not equal for each of the particles. Thus, to make analysis possible we would like to define a quantity independent of it: Diffusion Constant $\times$ surface area. The quantity is multiplied for the following reasons. The greater the surface area the greater the likelihood that any area on the particle would be hit by water molecules. However, this also means that the larger the surface area, the lower the probability that the any one direction has more particles hitting it than any other. This notion can also be observed in the Stokes–Einstein equation (explained in the next section). This equation is not invoked here because it describes spherical particles. However, it can be understood that our idea conforms to this. Table II. displays these values (values have a factor $10^{-6}\frac{m^4}{s}$ multiplied to them)

The diffusion constant reflects the ease with which a particle is displaced from its position due to Brownian forces. Since the values presented in Table II.

Table II. Diffusion Constant x surface area for the Particles

Sr. No	Name of Particle	Diffusion Constants
1	Peanut	14.75
2	Pear	161.85
3	Snowman	43.91

have already been adjusted for surface area, and all other determining factors such as temperature, density, viscosity of liquid are all uniform, it must be that these values are reflective of how the geometry and construction of these particles affects their Brownian motion.

The data indicates to us that the pear particle has the highest value for this quantity. It is possible to understand this by scrutinizing the geometry of the particle. This particle can be considered to be the least symmetric of all the particles, because it deviates most from the spherical models and the two different sides of the particle have objects with vastly different radii. This allows there to be disparities between the number of particles hitting in different directions, allowing the particle to be translated easily.

Next, the snowman particle has the second highest value for the compound quantity. The snowman particle consists of two spheres with a large difference in the radii of the two. For this reason, most of the larger sphere observes spherical symmetry, i.e. for most directions it is likely for the same number of water molecule to be hitting the exactly opposing direction at any given instant. Nevertheless, the smaller sphere causes some asymmetry to be introduced. Therefore, this particle has has a value lower than that of the pear particle but still larger than the next particle.

The peanut particle is the last of the particles investigated in the study, and it is no surprise that this particle has the most symmetric structure of all of the particles. The peanut particle enjoys symmetry in the form of diametrically opposite directions having equal likeliness of particles hitting. It is not as symmetric as a perfect sphere, but it definitely enjoys more symmetries than the snowman and pear particles.

VI. ERROR ANALYSIS

For the purpose of error analysis observations from the Brownian motion of a spherical particle are to be used. Before the investigation was undertaken with the three particles, a spherical was used to be able to determine the accuracy of the equipment and the setup. The Stokes–Einstein equation suggests the following about diffusion of spherical particles through a liquid with a low Reynolds number[6]:

$$D = \frac{K_B T}{6\pi\eta r} \tag{28}$$

Where D is the diffusion constant, T is the absolute temperature, K_B is the Boltzmann's constant, η is the dynamic viscosity, and r is the radius of the spherical particle. Still water satisfies the condition that the liquid have a low Reynolds number, so the aforementioned expression can be utilized. Since all the investigations were undertaken in the identical conditions (including identical temperature), it is possible to use the accuracy with which the Boltzmann's constant can be determined for the spherical particles to comment on the reliability of the data availed for the other experiments. The following images show the graph for the mean square displacement of the spherical particle against the time step sizes:

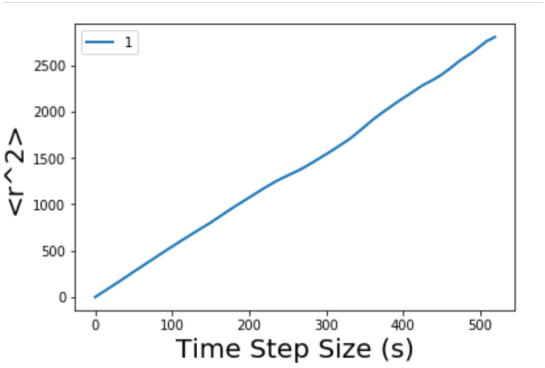

Figure 26. Graph Displaying Mean Square Displacement against Time Step size for Spherical Particle

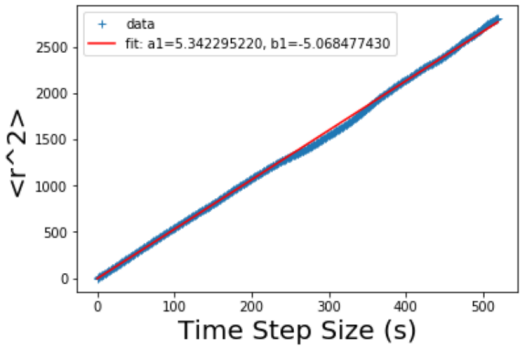

Figure 27. Graph Displaying Mean Square Displacement against Time Step size for Spherical Particle along with Linear Regression

With the value of the slope, the Boltzmann constant has the following the value: $K_B = 1.422 \times 10^{-23} \frac{J}{K}$. This

corresponds to an error of approximately 2.99%. This is a sufficiently low deviation that the result produced from the experiments can be deemed reliable.

VII. EVALUATION AND DISCUSSION

This section serves as a reflection on the various elements of the investigation and the report.

A. Polymer Density

In the certificate if analysis provided by the manufacturer of the particles (they refer to them as Microspheres), there is some very important information about the properties of the particles. Amongst these is the polymer density. The document states that the density of the polymer used is 1.05 g/ml. This is 0.05 g/ml higher than that of the distilled water used as the medium for Brownian motion.

It would be ideal to have a polymer that has a density identical to that of distilled water used for the purpose of manufacturing the particles. The denser particle would be more likely to move in one direction and out of focus. However, this is difficult to come across. Furthermore, it is better to have a polymer that is slightly denser than the liquid as opposed to slightly less dense. A less denser particle would rise to the surface and its motion is more likely to be affected by drift occurring due to evaporation. The difference in density is small enough to justify using the particles for an investigation.

B. Presence of Sodium Azide

The certificate of analysis also states that the the solution containing the particles also contains 0.09 % or less Sodium Azide. This compound is most notable for its use in commercial Airbags for the purpose of inflating them on incident. Nevertheless, it is also often used as a preservative, and it seems that this is the purpose that it satisfies in the solution.

Another feature of Sodium Azide is that it is acutely toxic. Sodium azide has caused deaths for decades. It has been given the NFPA 704's highest rating of 4 on the health scale. It may be fatal even in contact with skin or if swallowed. Even minute amounts can cause symptoms. It is known to produce extrapyramidal symptoms with necrosis of the cerebral cortex, cerebellum, and basal ganglia.[7] Therefore, waste disposal becomes crucial. All the discarded slides were very carefully placed in Bio-hazard waste bins. Even while conducting the investigations, precautions were taken: slides were always handled with gloves on.

VIII. EXTENSIONS TO THE INVESTIGATION

There are many possible extensions to the investigation that has been carried out for the purpose of this report. There are several other particle shapes that can be investigated. This would include rod-like structures (to emulate rod-shaped bacteria, to understand their motion *sans* their flagella), long and thin fibre-like structures (to emulate fibrous agents like Asbestos), and the list goes on.

Apart from separate shapes it also possible to employ different liquids to emulate motion in bodily fluids, for example. Liquids such as brine could be useful. Similarly, using liquids that have the same properties as blood can further help understand motion in the particular liquid.

Appendix A: Note on Einstein's Model

The description of Brownian motion in Einstein's 1905 work relies on the assumption of the existence of a time-interval τ, such that the particle's motion during different τ -intervals is independent. The coarse-grained version of this motion leads then to the known diffusion equation.

However, in many cases this assumption is violated. An example is dispersive transport in disordered systems which stems from a broad distribution of waiting times which may have a diverging mean. This ill-defined mean waiting time results in subdiffusion. In this contribution we derive, within a unified scheme, two equivalent forms of kinetic equations for subdiffusive behavior. For power-law waiting-time distributions, the equations reduce to the "normal" form of a fractional Fokker-Planck equation with a fractional derivative replacing the first-order time-derivative, or to a "modified" form. [8]

For waiting time distributions which are not pure power laws one or the other form of the kinetic equation are shown to be advantageous, depending on whether the process slows down or accelerates in the course of time.

Langevin in 1908 introduced an approach based on what nowadays is called stochastic differential (or Langevin) equation, which was claimed to be "infinitely simpler". This was also presented in the paper to serve as an alternate explanation to the derived expression. It is necessary to recognize the limitations of Einstein's postulates, and this appendix serves to show that this knowledge is not foregone.

Appendix B: Python Code

After the files have been read and the point-wise displacements (r1, in this case) from the origin has been determined, the following section is used to calculate the mean square displacement for an individual particle and visualize it:

```
c1 = np.zeros(len(r1))
s1 = np.zeros(len(r1))

for j in range(1, len(r1)):
    for i in range(1,len(r1)-j):
        s1[i] = r1[j+i] - r1[i]
    c1[j] = sum(s1)/(len(r1)-j)
    s1 = np.zeros(len(r1))

plt.plot(n1,c1, label = "1", linewidth = "2")
plt.xlabel("Time Step Size (s)", size = 20)
plt.ylabel("<r^2>", size = 20)
plt.legend()
plt.show()
```

This next section shows how the average values for each individual particle are taken and then used for data visualization. This also includes the linear regression method:

```
cn = (c1+ c2 + c3 + c4 + c5 + c6 + c7 + c8 + c9 +
    c10 + c11 + c12 + c13 + c14 + c15 + c16)/16

plt.plot(n,cn, label = "1", linewidth = "2")
plt.xlabel("Time Step Size (s)", size = 20)
plt.ylabel("<r^2>", size = 20)
plt.legend()
plt.show()

def func1(n, a1, b1):
    return a1*n + b1

popt1, pcov1 = curve_fit(func1, n, cn)

plt.plot(n, cn, '+', label='data')
plt.plot(n, func1(n, *popt1), 'r-', label='fit:
    a1=%5.9f, b1=%5.9f' % tuple(popt1))
plt.xlabel("Time Step Size (s)", size = 20)
plt.ylabel("<r^2>", size = 20)
plt.legend()
plt.show()
```

Appendix C: Software Information

1. ImageJ is a public domain Java image processing program inspired by NIH Image for the Macintosh. It runs, either as an online applet or as a downloadable application, on any computer with a Java 1.4 or later virtual machine. Downloadable distributions are available for Windows, Mac OS, Mac OS X and Linux.

   It can display, edit, analyze, process, save and print 8-bit, 16-bit and 32-bit images. It can read many image formats including TIFF, GIF, JPEG, BMP, DICOM, FITS and "raw". It supports "stacks", a series of images that share a single window. It is multithreaded, so time-consuming operations such as image file reading can be performed in parallel with other operations.

   It can calculate area and pixel value statistics of user-defined selections. It can measure distances and angles. It can create density histograms and line profile plots. It supports standard image processing functions such as contrast manipulation, sharpening, smoothing, edge detection and median filtering.

   It does geometric transformations such as scaling, rotation and flips. Image can be zoomed up to 32:1 and down to 1:32. All analysis and processing functions are available at any magnification factor. The program supports any number of windows (images) simultaneously, limited only by available memory.

   Spatial calibration is available to provide real world dimensional measurements in units such as millimeters. Density or gray scale calibration is also available.

   ImageJ was designed with an open architecture that provides extensibility via Java plugins. Custom acquisition, analysis and processing plugins can be developed using ImageJ's built in editor and Java compiler. User-written plugins make it possible to solve almost any image processing or analysis problem.

   ImageJ is being developed on Mac OS X using its built in editor and Java compiler, plus the BBEdit editor and the Ant build tool. The source code is freely available. The author, Wayne Rasband (wayne@codon.nih.gov), is at the Research Services Branch, National Institute of Mental Health, Bethesda, Maryland, USA.

   Schneider, C. A.; Rasband, W. S. & Eliceiri, K. W. (2012), "NIH Image to ImageJ: 25 years of image analysis", Nature methods 9(7): 671-675.

2. Leica LAS EZ software. © 2020 Leica Microsystems.

Leica Microsystems is a leading global developer and manufacturer of innovative high-tech optical precision systems for the analysis of microstructures. Leica Microsystems is one of the market leaders in the fields of microscopy, confocal laser microscopy and corresponding image analysis, sample preparation of microscopic objects and medical technology. The company manufactures a wide range of products for a variety of applications that require microscopic visualization, measurement and analysis. The range includes system solutions in the field of life science including biotechnology and medicine as well as materials science and industrial quality control. With 13 production sites in eight countries, sales and service companies in 19 countries and an international dealer network, the company operates in more than 100 countries. Global management is based in Wetzlar, Germany.

3. Micro-Manager is an Open Source software package for controlling automated microscopes on multiple platforms (Windows, Mac and Linux). The software is being developed in the Vale Lab at the Unversity of California San Francisco and funding was provided by the Sandler Foundation and a grant from the NIH. The original software design was by Nenad Amodaj, and the software is currently developed by Arthur Edelstein and Nico Stuurman. Many individuals contributed source code or other types of help (including this documentation). The Micro-Manager source code is distributed under the BSD license for the user interface and the LGPL license for the MMCore (control module). Most supplied device drivers ('adapters') for cameras and other devices are covered by the BSD license. Copyright for some of the adapters is owned by other parties.

[1] D. Tabor, Gases, liquids and solids and other states of matter (Cambridge University Press, 1995) p. 120.

[2] F. Reif, Fundamentals of statistical and thermal physics (Levant Books, 2010).

[3] A. Einstein, Investigations on the theory of the Brownian movement (Dover Publications, 1956).

[4] Bekman, S. (n.d.). Retrieved from https://stason.org/TULARC/recreation/photography/lenses-faq/31-What-do-APO-and-Apochromatic-mean.html.

[5] Introduction to Microscope Objectives. (n.d.). Retrieved from https://www.microscopyu.com/microscopy-basics/introduction-to-microscope-objectives.

[6] N. W. Ashcroft and N. D. Mermin, Solid State Physics (Cengage Learning, 1976) p. 826.

[7] Northeastern University. (n.d.). Sodium Azide. Retrieved from https://www.northeastern.edu/ehs/ehs-programs/hazardous-waste-management/fact-sheets/sodium-azide/.

[8] Sokolov, I. M., Klafter, J. (2005). From diffusion to anomalous diffusion: A century after Einstein's Brownian motion. Chaos: An Interdisciplinary Journal of Nonlinear Science, 15(2). doi: 10.1063/1.1860472.

[9] G. A. . J. T. Lin Tian, Brownian diffusion of fibers, Aerosol Science and Technology **50:5**, 474 (2016).

[10] K. R. S. t. J. W. Gentry and J. Schrmann, The diffusion coefficients for ultrathin chrysotile fibers, Journal of Aerosol Science **7**, 869 (1991).

[11] G. P. Berman, Jr. and F. M. Izrailev, Jr., The electrical mobilities and scalar friction factors of modest-to-high aspect ratio particles in transition regime, Journal of Aerosol Science **82**, 24 (2015).

[12] E. Hinch and L. Leal, The effect of brownian motion on the rheological properties of a suspension of non-spherical particles, Journal of Fluid Mechanics **52:4**, 683 (1972).

[13] I. A. Lasso and P. D. Weidman, Stokes drag on hollow cylinders and conglomerates, Physics of Fluids **29:12**, 3921 (1986).

[14] H. Ounis and G. Ahmadi, A comparison of brownian and turbulent diffusion, Aerosol Science and Technology **13:1**, 47 (2007).

[15] M. G. Sabine Tran-Cong and E. E. Michaelides, Drag coefficients of irregularly shaped particles, Powder Technology **139**, 21 (2004).